Article

Experimental Measurement and Numerical Modelling of Solid Network-Based Schoen's I-Graph—Wrapped Package (I-WP) toward Cooling Heat Sink

M. Yahya [1], A. Yahya [2] and M. Z. Saghir [1,*]

[1] Department of Mechanical, Mechatronics and Industrial Engineering, Toronto Metropolitan University, Toronto, ON M5B 2K3, Canada
[2] College of Science, University of Duhok, Duhok 42001, Iraq
* Correspondence: zsaghir@torontomu.ca

Abstract: Triply Periodic Minimal Surfaces (TPMS) are periodic implicit surfaces with zero-mean curvature. Zero-mean surfaces are those that locally have minimum surface area for a given boundary. This study investigates the thermal performance of a TPMS geometry, Schoen's I-graph Wrapped Package (I-WP), for application as a compact heat sink. While most prior work focuses on gyroid-based TPMS structures, this research explores the less-studied I-WP architecture fabricated from copper with a fixed porosity of 0.7. The influence of unit cell size on convective heat transfer and flow resistance is examined both experimentally and numerically. Experimental testing was conducted for unit cell sizes of 4 mm, 6 mm and 8 mm, while numerical simulations using COMSOL Multiphysics extended the analysis to sizes of up to 14 mm. Strong agreement between the measured and simulated results (within a 3% temperature deviation and 7% for the local Nusselt number) validated the numerical model. Empirical correlations for the average Nusselt number were developed based on both experimental and numerical data. The novelty of this paper lies in the performance of the experiment for different flow rates and unit cell sizes. The study identified 12 mm as the optimal unit cell size, yielding the highest Performance Evaluation Criterion (PEC) and demonstrating an effective balance between thermal enhancement and hydraulic performance. Furthermore, uniform temperature distributions observed across the flow direction underscore the advantages of TPMS structures over conventional metal foams. These findings establish the I-WP geometry as a promising candidate for next-generation, geometrically tunable heat exchangers that can be enabled by additive manufacturing.

Keywords: TPMS; I-WP; heat sink; experimental measurement; heat enhancement; CFD; optimization

1. Introduction and Literature Review

Triply Periodic Minimal Surfaces (TPMS) are geometric structures that repeat periodically in all three spatial directions and exhibit equal surface curvature in three directions. Their distinctive structure provides a high specific surface area, making them highly effective for maximizing heat transfer between adjacent regions and improving thermal efficiency. The shape and complexity of TPMS can be precisely controlled through the parameters of their implicit equations, enabling highly customizable thermal system designs. By modifying the parameters of the implicit equations, a variety of TPMS structures can be generated, each with distinct geometric and functional properties [1]. TPMS structure could be found in nature, whether in insect bodies, chemistry, or other engineering applications. More interest is rising in using such structures in cooling surfaces. Their advantage
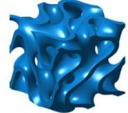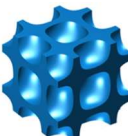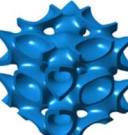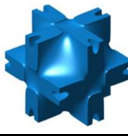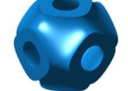
is that they provide uniform cooling and are lightweight [1]. The new heat exchanger model, which incorporates a TPMS structure, is an example of an engineering application in the aerospace industry [2,3]. TPMS structures, widely utilized in additive manufacturing, are generally classified into two primary types: sheet network and solid network structures. These types encompass a range of topologies, such as gyroid, diamond, I-WP, Fischer-Koch S and primitive, among others. TPMS structures, characterized by their unique geometries and mechanical properties, offer versatile opportunities for designing and fabricating advanced materials and functional devices [4].

Level-set equations describe surfaces implicitly using a scalar function $\Phi(X, Y, Z)$, where the surface of interest is defined by the condition $\Phi(X, Y, Z) = c$, with c being a constant iso-value that determines the exact shape and topology of the surface. The resulting surface, often referred to as an iso-surface, represents the set of all points (X, Y, Z), that satisfy this equality. In contrast, $X = 2\pi x, Y = 2\pi y,$ and $Z = 2\pi z$ represent Cartesian coordinates that define the three-dimensional spatial framework of the surface. Table 1 presents examples of TPMS forms and their corresponding mathematical expressions, which are commonly used in the literature and formulated using trigonometric or algebraic expressions, allowing for the representation of complex geometries in a compact mathematical form [3,5].

Table 1. Common level-set equations and their corresponding iso-surfaces [3].

Pattern Name	Visualization	Mathematical Function
Gyroid		$\Phi(X, Y, Z) = \cos(X).\sin(Y) + \cos(X).\sin(Z) + \cos(Z).\sin(X) = 0$
Fischer-Koch S		$\Phi(X, Y, Z) = \cos(2X)\sin(Y)\cos(Z) + \cos(2Y)\sin(Z)\cos(X) + \cos(2Z)\sin(X)\cos(Y) = 0$
Schwarz Diamond (D)		$\Phi(X, Y, Z) = \sin(X).\sin(Y).\sin(Z) + \sin(X).\cos(Y).\cos(Z) + \cos(X).\sin(Y).\cos(Z) + \cos(X).\cos(Y).\sin(Z) = 0$
Fliickenstuck-Reiche F-RD		$\Phi(X, Y, Z) = \cos\cos(2X)\sin\sin(Y)\cos\cos(Z) + \cos\cos(X)\cos\cos(2Y)\sin\sin(Z) + \sin\sin(X)\cos\cos(Y)\cos(2Z)$
I-WP		$\Phi(X, Y, Z) = 2[\cos(X).\cos(Y) + \cos(Y).\cos(Z) + \cos(Z).\cos(X)] - \cos(2X) - \cos(2Y) - \cos(2Z) = 0$
Neovius		$\Phi(X, Y, Z) = 3(\cos(X) + \cos(Y) + \cos(Z)) + 4\cos(X)\cos(Y)\cos(Z) = 0$
Schwarz Primitive (P)		$\Phi(X, Y, Z) = \cos(X) + \cos(Y) + \cos(Z) = 0$

Baobaid et al. investigated the natural convection performance of TPMS-based heat sinks, including the Diamond-Solid, Gyroid-Solid, and Gyroid-Sheet networks [5]. Using CFD analysis, they found that TPMS designs, especially the Gyroid-Sheet, outperformed traditional pin-fin and foam heat sinks, with high heat dissipation. The study also demonstrated that structural orientation and enclosure conditions have a significant impact on performance and that radiation can substantially contribute to total heat transfer.

Su et al. demonstrated that 3D-printed stainless steel heat exchangers with TPMS structures (Diamond and Gyroid) outperform conventional PCHEs in micro gas turbines, with over four times higher Nusselt numbers and

effectiveness [6]. Despite higher pressure losses, their thermal performance and power density were significantly better, especially at smaller lattice sizes, making TPMS a promising solution for compact, high-efficiency heat exchangers.

Wang et al. used CFD to evaluate the thermal-hydraulic performance of TPMS-based heat exchangers for advanced nuclear systems like ADS [7]. Comparing I-WP and Primitive topologies with a conventional PCHE using LBE and Helium, they found TPMS designs achieved two to three times higher heat transfer with half the volume. The study underscores TPMS's potential to enhance nuclear heat exchanger efficiency and compactness. Tang et al. investigated the heat transfer performance of TPMS structures, specifically those of the Gyroid, Diamond, and IWP types, using simulations and experiments with air as the working fluid [8]. They found TPMS designs, especially the Diamond type, significantly improved heat transfer over traditional fins, with up to 196% higher Nusselt numbers. Despite increased pressure drop, the overall performance was better, making TPMS a strong candidate for compact, efficient heat sinks.

Gandy et al. discussed different types of TPMS structures, including the IWP structure [9]. They highlighted mathematically the formulation of each TPMS. They also provided detailed mathematical approximations for the P, G, D, and I-WP using nodal surface equations. Their work established foundational analytical descriptions for these complex geometries, enabling their accurate modelling and facilitating their application in materials science and engineering, particularly for designing advanced porous structures and multifunctional materials. Kobayashi et al. studied the I-WP minimal surface-based photonic crystal [10]. The crystal's unique asymmetry and (110) orientation explain the beetle's green coloration via a photonic bandgap, and the presence of twin domains suggests a distinct developmental mechanism.

In contrast to a gyroid or diamond structure found in Butterfly and weevil scales, the I-WP structure is found in longhorn beetles. Al-Ketan et al. investigated the relationship between architectural property and the possible creation of Schoen's I-WP minimal surface to create a lattice structure [4]. They presented experimental and computational evidence of the robustness and suitability of sheet-based I-WP structures for various engineering applications that require strong and lightweight materials with high energy absorption. Their findings confirmed that such a structure exhibits a near-stretching-dominated stiffness and deformation behaviour, as well as bending behaviour. They concluded that such a structure demonstrated that stiffness and strength values could reach more than double those obtained for strut-based and skeletal-based lattice structures.

Montazerian et al. focused their research on the effect of pore architecture and porosity in radial and longitudinal fluid flow directions [11]. They found that I-WP TPMS-based scaffolds are generally more permeable than lattice-based scaffolds along the flow direction.

Most of Schoen's I-WP minimal surface structure research focused on its strength, flexibility, and mechanical properties. Ahmed et al. conducted a numerical modelling to investigate the effect of residual stresses on the mechanical properties of IN718 triply periodic minimal surface lattices fabricated using selective laser melting (SLM) for different relative densities [2]. Amongst the structures, I-WP was used in their analysis. The residual stresses on the elastic module for Schoen I-WP were found to be significant, but they were less critical in terms of yield strength. Recently, Tang et al. utilized the I-WP structure to investigate the convective heat transfer process and evaluate its performance criteria [12].

Previous research has focused on the benefits of using I-WP due to its structural flexibility and high Young's modulus. Among the three different structures, diamond has the best heat transfer coefficient. Its geometric structure, without through-holes, led to a more substantial wall disturbance to the fluid, thereby enhancing heat transfer. However, it is essential to note that the authors used a sheet-based TPMS structure, not a solid-based structure. Air is used as a circulating fluid, and heating is done using a steam generator.

Zhang et al. investigated the vibrational properties of the I-WP and found that this structure exhibits suitable vibration isolation properties [13]. They discovered that additively manufactured I-WP type TPMS lattice structures, made via selective laser melting, exhibit superior mechanical properties and vibration isolation compared to conventional BCC lattices. Their results show that increasing volume fraction and reducing cell size enhance stiffness and natural frequency. In contrast, lower volume fractions and larger cells are better for low-frequency vibration damping, making I-WP type TPMS lattices promising for lightweight, load-bearing, and vibration-isolating applications. Men et al. investigated a method to enhance the thermal performance of the I-WP structure in relation to the cooling heat sink [14]. The proposed model establishes a relationship between the porosity and its effective parameters. The optimization employed a density-based approach by treating the I-WP as distinct materials. Their findings indicated that the I-WP pressure drop decreased. They demonstrated the effectiveness of combining a porous media model with topology optimization of the I-WP TPMS model.

Rajkumar et al. provided the foundations for designing a scaffold based on the I-WP TPMS unit cell for application in new bone structures [15]. Additional work on using I-WP for energy storage is presented by [7,16]. Ouda et al. developed static mixers based on TPMS and compared them to conventional Kenics mixers [17]. TPMS designs,

notably Diamond, Gyroid, and I-WP, offered similar or better mixing efficiency with significantly lower energy consumption, mainly when used in hybrid or modified configurations. Yeranee and Rao reviewed recent studies on the use of TPMS structures, including Gyroid, Diamond, Primitive, and IWP, in cooling channels [18]. The review highlights how TPMS design variables (e.g., porosity, wall thickness, and unit cell size) significantly influence flow behaviour and heat transfer performance. Compared to traditional structures, TPMS geometries offer enhanced thermal conductivity, better mixing, and reduced pressure loss, making them effective for heat sinks and compact heat exchangers.

The reviewed literature highlights significant progress in modelling, simulating, and applying TPMS across various domains, particularly in heat exchangers, static mixers, energy storage, and biomedical scaffolds. The literature reveals TPMS, particularly structures like Gyroid, Diamond, and I-WP, have emerged as powerful geometries for advanced thermal and structural applications due to their unique mechanical, thermal, and morphological properties. While Gyroid and Diamond structures are frequently studied for heat transfer enhancement, the I-WP topology stands out primarily for its superior mechanical strength, permeability, and vibration damping. Although recent studies have begun exploring the thermal potential of I-WP-based designs, a notable gap remains in experimental research validating their performance in cooling systems.

This review reveals that the majority of I-WP TPMS investigations have centred on structural mechanics such as stiffness, energy absorption, and vibrational behaviour (e.g., [2,4,13]), with few experimental studies focused on its thermal performance. Among the reviewed works, only a limited number (e.g., [14]) examined I-WP in cooling contexts, and most of these relied on numerical simulations rather than empirical validation, underscoring a research gap in experimental thermal characterization of I-WP-based heat exchangers and heat sinks.

Based on the reviewed literature, this study presents a novel experimental investigation of cooling hot surfaces using the I-WP TPMS structure, with a specific focus on the impact of unit cell size. To the best of our knowledge, this represents the first experimental validation of the I-WP structure's thermal performance, addressing a notable gap in existing research. The experimental results are further compared with numerical simulations, demonstrating strong agreement and reinforcing the reliability of the computational model.

2. Experimental Description

TPMS are periodic implicit surfaces with zero mean curvature. Zero-mean surfaces are those that locally have minimum surface area for a given boundary. The TPMS is composed of multiple surfaces in the three principal directions. Thus, the TPMS network is a repeated lattice structure. Saghir et al. numerically analyzed heat exchangers using various TPMS structures under forced convection and found enhanced thermal performance due to their flow-optimizing geometries [19,20]. The study highlights TPMS as a promising candidate for efficient, lightweight heat exchangers, offering improved heat extraction and more uniform temperature distribution.

The present study focuses on the use of a solid-based Schoen's I-graph–Wrapped Package (I-WP) structure, commonly referred to as the I-WP TPMS structure. This structure was manufactured using 3D printing by [4]. This specific TPMS geometry is characterized by its continuous, periodic surface with minimal mean curvature, offering advantageous mechanical and thermal properties. The level set equation representing the Schoen I-WP structure is expressed as follows:

$$\Phi(X, Y, Z) = 2[(2\alpha\pi x).\cos(2\beta\pi y) + \cos(2\beta\pi y)\cos(2\gamma\pi z) + \cos(2\gamma\pi z).\cos(2\alpha\pi x)] \\ - \cos2(2\alpha\pi x) - \cos2(2\beta\pi y) - \cos2(2\gamma\pi z) = c \tag{1}$$

where α, β, and γ denote constants related to the unit cell size in the x, y and z direction, respectively. On the other hand, c is the offset parameter, which is equal to zero for a single cell of the TPMS. The TPMS-based lattices can be constructed using two methods based on minimal surfaces and are typically categorized into two main types: solid-based TPMS lattices, also referred to as solid networks, and sheet-based TPMS lattices, known as sheet networks. Solid-based TPMS structures are characterized by their interconnected, continuous solid regions, making them particularly suitable for applications requiring high strength, stiffness, and efficient heat transfer. In contrast, sheet-based lattices consist of thin surfaces and are often used where lightweight structures and high surface-area-to-volume ratios are desired.

In the present study, a solid-based TPMS lattice is employed to investigate the thermo-fluidic performance of Schoen's I-graph–Wrapped Package (I-WP) geometry. Both experimental and numerical analyses are conducted to evaluate its performance under controlled conditions. The experimental setup used in this study is illustrated in Figure 1. It consists of a comprehensive arrangement that includes a data acquisition system, flow meters, circulating pumps, thermocouples for temperature monitoring, and cooling towers to maintain controlled inlet conditions. This setup is designed to replicate realistic flow and thermal conditions, ensuring accurate validation of the numerical simulations. To maintain consistency with established methodologies, the experimental

configuration follows the approach detailed in [19,20]. This foundational setup provides the basis for assessing the influence of TPMS geometry, specifically the I-WP structure, on heat transfer performance and flow behaviour.
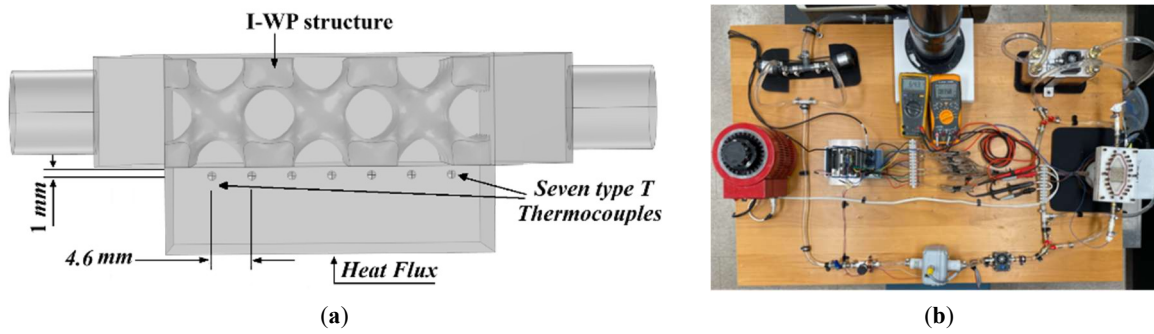

Figure 1. Experimental setup. (**a**) the experiment setup; (**b**) location of the seven thermocouples.

In this investigation, the I-WP structure has a constant porosity of 0.7, and three different unit cell sizes (4 mm, 6 mm and 8 mm) are tested to assess the influence of geometric scaling on heat transfer performance. The TPMS structure is heated from below using an aluminum block, simulating realistic heat flux conditions. Temperature measurements are recorded 1 mm beneath the TPMS/aluminum block interface, as depicted in Figure 1b, allowing for precise monitoring of thermal behaviour at the interface. For comsprehensive details regarding the experimental apparatus and methodology, the reader is referred to the work by [19,20], which provides an in-depth description of the instrumentation, flow loop, and measurement protocols employed. This configuration serves as the basis for validating numerical simulations and analyzing the thermofluidic behaviour of I-WP TPMS structures under varying conditions.

The three TPMS under investigation are displayed in Figure 2 and are made of copper. The flow rates applied in the experiments are 11.8 cm³/s, 15.73 cm³/s and 19.85 cm³/s, respectively. This corresponds to an inlet velocity of 0.15 m/s, 0.2 m/s and 0.25 m/s, respectively. This will maintain a laminar flow circulation during the investigation. The heat flux applied at the bottom of the aluminum block is kept constant during the entire experiment and set to 38.4KW/m². After each run, the circulating fluid, in this case water, is cooled to approximately 10 °C before the experiment is restarted. For each case, three runs are performed, and sensitivity analysis has been determined and explained in detail in reference by [19,20]. A thermo-paste is added between the TPMS structure and the aluminum block to achieve excellent contact between the two structures under investigation. The test chamber, shown in white, is made of Teflon material, which is known to be a good insulator, preventing extensive heat leaks into the environment.
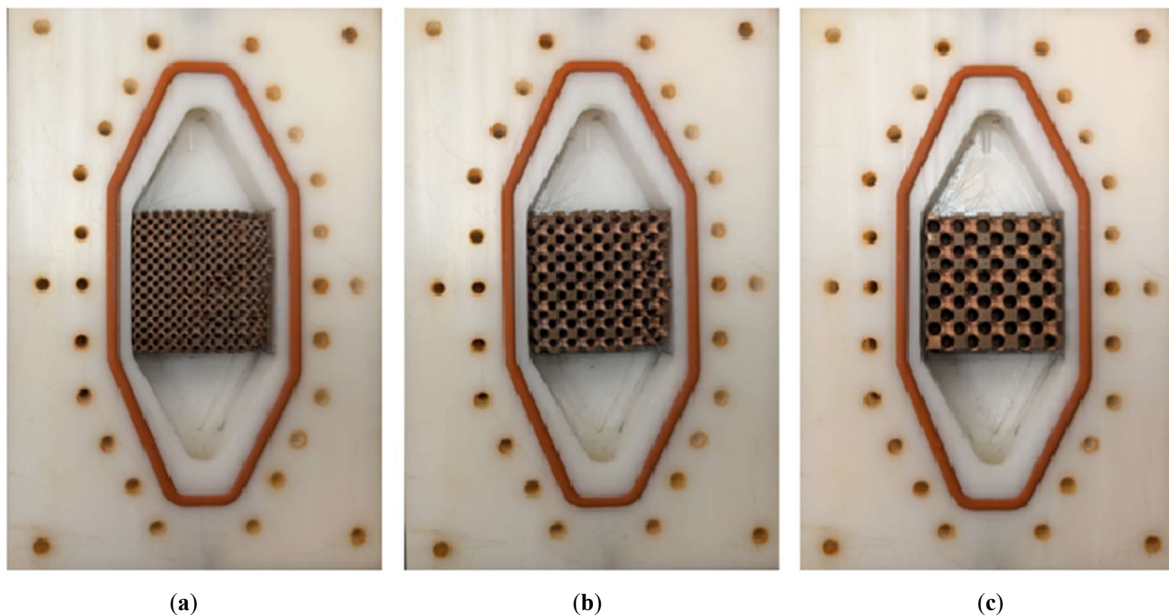

Figure 2. I-WP structure location in the test chamber. (**a**) UC = 4 mm; (**b**) UC = 6 mm; (**c**) UC = 8 mm.

Figure 2 presents the three TPMS structures, each with a unit cell of 4 mm, 6 mm, and 8 mm, respectively, inside the test section.

The experimental procedure begins by first establishing a steady-state inlet temperature. The working fluid, water, is circulated through the system without heat input using a temperature-controlled water bath. This pre-conditioning phase continues until the inlet water temperature is stabilized at approximately 10 °C, ensuring consistent initial conditions across all test runs.

Once this temperature threshold is reached, the prescribed heat flux is applied to the bottom surface of the aluminum heating block, which is in contact with the TPMS specimen.

Following the application of heat flux at the bottom of the aluminum block, the system is carefully monitored until a new thermal steady state is achieved. Details on the experimental procedure can be easily found in References [19,20]. This is determined by observing the temperature readings from multiple thermocouples embedded in the system, ensuring that fluctuations remain within an acceptable margin of error. Once thermal stability is confirmed, data acquisition is initiated. Temperature data from each thermocouple is recorded continuously for a period of 10 min, allowing for the determination of an accurate time-averaged temperature at each measurement location. After the data collection period, the heat flux is turned off, and the system is allowed to cool.

The working fluid continues to circulate through the water reservoir until the inlet temperature once again approaches 10 °C, thereby restoring the baseline condition. This process is repeated for each test case, with three independent runs conducted per configuration to ensure repeatability and statistical reliability. For each case, the average temperature readings from the three trials are used for analysis. Throughout all experiments, the porosity of the TPMS structures is maintained at 0.7, ensuring that comparisons between different unit cell sizes are based solely on geometric variations, rather than changes in material volume or flow resistance. This rigorous experimental protocol is designed to yield reliable, reproducible measurements for evaluating the thermal performance of the I-WP TPMS structure under well-defined boundary conditions.

Table 2 presents the average temperature distribution harvested at three flow rates for the three TPMS shown in Figure 2. Figure 3 displays the temperature variation from Table 2 at each thermocouple location. Although the non-uniform temperature distribution is shown in Figure 3, this is because of the scaling of the temperature axis.

Table 2. Experimental data of the temperature for different flow rates and unit cell sizes.

| Flow Rate (cm³/s)	UC (mm)	Temperature in °C at Different Thermocouple Positions (mm)							Tin (°C)
		4.2	8.4	12.6	16.8	21	25.2	29.4	
11.80	4	27.09	26.45	27.54	27.16	28.13	28.25	28.35	10.99
15.73	4	26.23	25.59	26.68	26.32	27.32	27.41	27.50	10.71
19.85	4	26.40	25.78	26.85	26.47	27.42	27.56	27.64	10.51
11.80	6	25.68	24.88	25.99	25.74	26.75	26.81	26.85	10.81
15.73	6	24.97	24.56	25.77	25.15	26.21	26.30	26.38	10.71
19.85	6	24.55	23.93	24.71	24.72	25.75	25.84	25.91	10.46
11.80	8	24.65	23.77	23.57	23.53	24.59	24.58	24.64	10.85
15.73	8	23.62	22.02	22.56	22.60	23.68	23.59	23.617	10.48
19.85	8	23.30	22.31	22.07	22.12	23.25	23.15	23.18	10.42
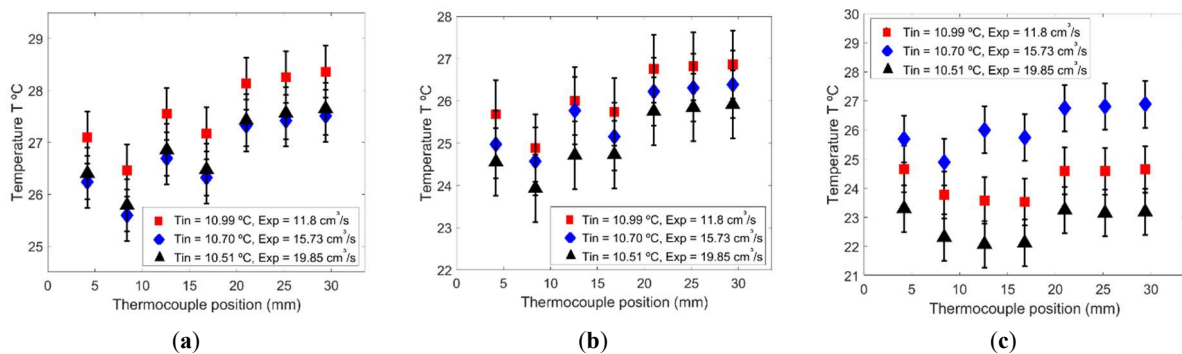
Figure 3. Experimental measurement of the temperature for different unit cells. (**a**) UC = 4 mm; (**b**) UC = 6 mm; (**c**) UC = 8 mm.

As presented in Table 2, the maximum temperature difference observed between the first thermocouple and the final thermocouple is 1.24 °C, representing a variation of approximately 4%. This minimal deviation is

indicative of a relatively uniform temperature distribution throughout the domain, which is critical for maintaining thermal stability in heat management applications.

For a unit cell size of 4 mm, a flow rate of 15.73 cm^3/s demonstrated superior cooling performance compared to the highest evaluated flow rate of 19.85 cm^3/s. This counterintuitive result suggests that higher flow rates may not necessarily yield better thermal performance, potentially due to reduced residence time within the heat exchange medium. Additionally, an increase in unit cell size leads to a more uniform temperature profile. This is primarily due to reduced hydraulic resistance and improved flow uniformity, which together enhance convective heat transfer.

One of the distinguishing features of employing TPMS structures rather than conventional metal foam materials is their inherent geometric regularity, which supports more predictable and uniform fluid flow. As a result, TPMS architectures contribute significantly to achieving a consistent temperature distribution, making them a promising design strategy for advanced thermal management systems.

Furthermore, the experimentally obtained local Nusselt number is presented in Table 3. A variation of approximately 7% is observed between the inlet region and the area near the outlet. This decline in the Nusselt number along the flow direction is indicative of the progressive development of the thermal boundary layer as the fluid traverses the domain.

The reduction in convective heat transfer performance downstream is characteristic of boundary layer thickening, which diminishes local temperature gradients and thus reduces the heat transfer coefficient. This effect is particularly pronounced in configurations with smaller unit cell sizes, where the flow exhibits increased complexity due to enhanced surface area and intricate geometrical features. In such cases, the initial segments of the flow path experience higher Nusselt numbers, attributed to the minimal thermal boundary layer and stronger thermal gradients at the onset of the TPMS structure. As the flow continues downstream, the boundary layer becomes more fully developed, leading to a reduction in local heat transfer rates.

Table 3. Experimental data of the Nusselt number for different flow rates and unit cell size.

Flow Rate (cm^3/s)	UC (mm)	Local Nusselt Number						
		4.2 (mm)	8.4 (mm)	12.6 (mm)	16.8 (mm)	21 (mm)	25.2 (mm)	29.4 (mm)
11.80	4	70.97	73.89	69. 52	70.64	66.66	66.18	65.80
15.73	4	73.60	76.78	71.52	73.19	68.80	68.41	68.04
19.85	4	71.92	74.81	69.93	71.58	67.57	67.03	66.68
11.80	6	76.83	81.19	75.25	76.54	71.66	71.39	71.21
15.73	6	80.14	82.47	75.88	79.12	73.71	73.27	72.90
19.85	6	81.08	84.84	80.18	80.10	74.74	74.29	73.95
11.80	8	82.77	88.44	89.78	90.09	83.15	83.22	82.85
15.73	8	86.96	99.02	94.60	94.24	86.55	87.13	86.99
19.85	8	88.71	96.09	98.04	97.68	89.07	89.76	89.51

These findings underscore the influence of TPMS geometry on local convective behaviour and highlight the importance of considering boundary layer evolution in the thermal design of such porous media systems.

Despite the observed variation, the local Nusselt number exhibits a consistent and uniform distribution along the flow direction. It is important to note that the local Nusselt number is inherently sensitive to fluctuations in temperature, which are represented by the convective heat transfer coefficient or the "thermal conductivity of fluid".

Even minor deviations in local temperature can significantly impact the computed Nusselt number, underscoring the importance of precise thermal measurements during experimentation. Given this sensitivity, the experimental data presented in Tables 2 and 3 serve not only to characterize the heat transfer performance of the TPMS structure but also to provide a critical benchmark for validating numerical simulations.These datasets offer valuable insight into the spatial distribution of convective behaviour. They can be used to assess the accuracy and predictive capability of computational models developed for TPMS-based heat exchangers or thermal management systems. Ensuring alignment between numerical and experimental results is essential for optimizing design parameters and improving the reliability of thermal performance predictions. Figure 4 presents the temperature distribution profiles for three distinct flow rates across three different TPMS unit cell sizes. Figure 4a is the temperature variation for a unit cell = 4 mm, Figure 4b for a unit cell = 6 mm, and finally Figure 4c for a unit cell = 8 mm.

The compiled data clearly illustrate that as the unit cell size increases, flow resistance decreases, allowing for more effective fluid circulation and enhanced convective heat transfer. This trend underscores the impact of geometric configuration on thermal performance within TPMS structures. Figure 5 shows the measured local Nusselt number at each thermocouple location. It is essential to notice that because the measured temperature is in

the denominator of the Nusselt number, any slight deviation is noticeable. Figure 5a shows the case of a unit cell of 4 mm, Figure 5b for a unit cell of 6 mm, and finally Figure 5c for a unit cell of 8 mm.
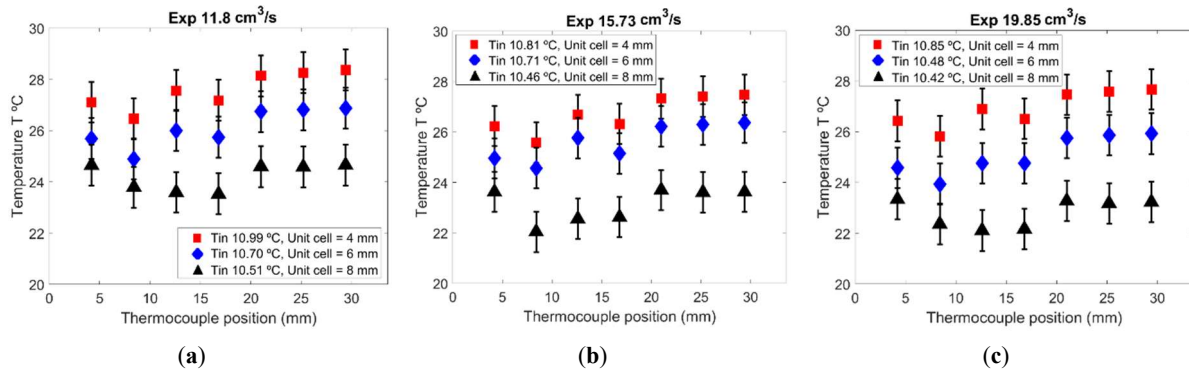

Figure 4. Experimental calculation of the temperature distribution profiles for each flow rate and for the three-unit cell. (**a**) 11.8 cm³/s; (**b**) 15.73 cm³/s; (**c**) 19.85 cm³/s.
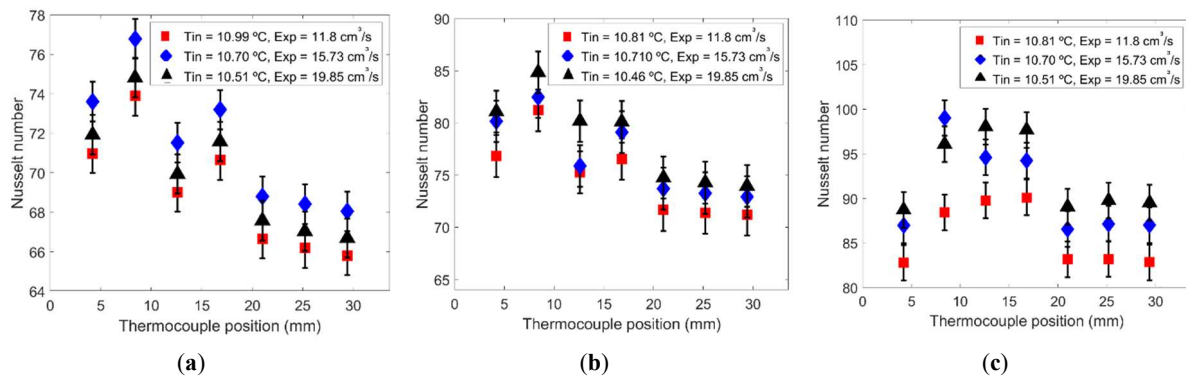

Figure 5. Experimental calculation of the local Nusselt number. (**a**) UC = 4 mm; (**b**) UC = 6 mm; (**c**) UC = 8 mm.

To quantitatively assess the relationship between thermal performance and key design parameters, a statistical correlation was developed based on experimental measurements obtained for the three-unit cell sizes. Specifically, the average Nusselt number was modelled as a function of unit cell size (denoted as UC in mm) and inlet velocity (u_{in} in m/s). Fisher's Analysis of Variance (ANOVA) was employed to evaluate the significance and interaction of these variables. The resulting regression model, expressed in Equation (2), captures the nonlinear dependence of the Nusselt number on both UC and u_{in}.

$$N_{u_{avg}} = f(u_{in}, UC)$$

$$N_{u_{avg}} = 71.8 - 8.32 \, UC + 119.19 \, u_{in} + 15.05 \, u_{in} \, UC - 428.57 \, u_{in}^2 \tag{2}$$

The accuracy of the model was validated by calculating the coefficient of determination (R^2), which confirmed a strong correlation without the need for adjustment. As shown in Equation (2), the fitted model accounts for the combined effects of geometric scaling and flow dynamics on heat transfer behaviour. Figure 6a compares the experimentally measured average Nusselt numbers to the values predicted by the regression model, demonstrating excellent agreement.

Figure 6b illustrates the three-dimensional surface plot of the predicted Nusselt number variation, further confirming the robustness of the proposed formulation. Overall, the strong alignment between the model and experimental data substantiates the predictive capability of the regression approach for optimizing TPMS-based heat exchanger designs.
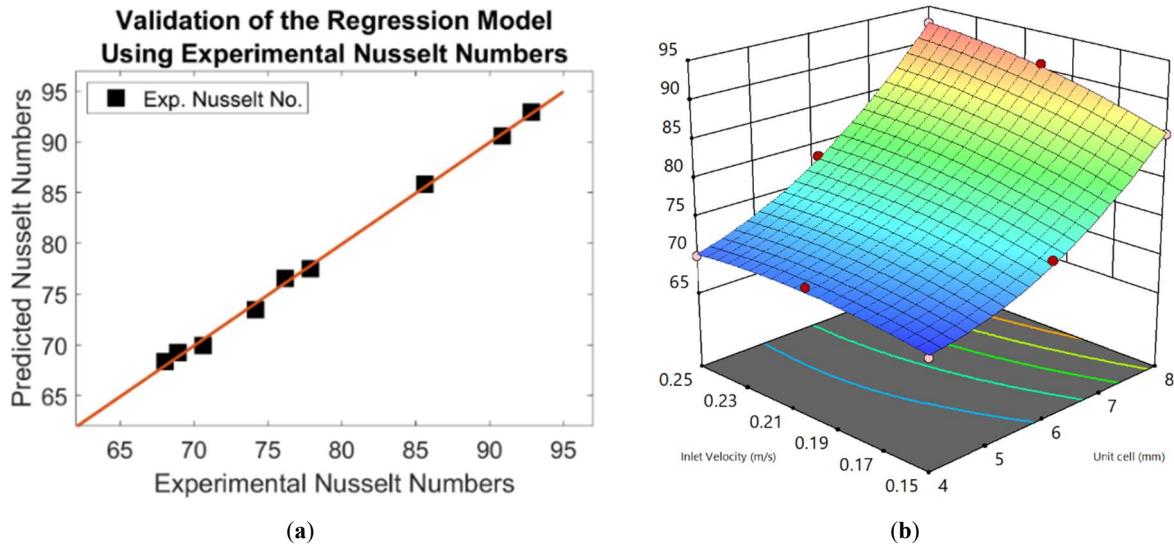
Figure 6. Fitted formulation for the average Nusselt number.

3. Comparison between Experimental Measurement and Numerical Modelling

3.1. Numerical Modelling

COMSOL Multiphysics finite element software [21] is used to simulate the experimental setup numerically. Using the finite element technique, the model is solved numerically by solving the continuity equation, the Navier-Stokes equation and the heat transfer formulation. Two non-dimensional parameters have been evaluated: the local Nusselt number (N_u), and the performance evaluation criteria (PEC).

3.1.1. Finite Element Formulation and Boundary Condition

The problem is solved numerically using the COMSOL software. The fluid is modelled as Newtonian, incompressible, and flowing under laminar conditions. The governing equations include the continuity equation and the Navier-Stokes equations for incompressible flow. The continuity equation is given by:

$$\nabla . \vec{V} = 0 \tag{3}$$

where $\vec{V}$ is the velocity vector, comprising components u, v and w, each expressed in m/s, in the $x, y,$ and z directions, respectively. The incompressible Navier-Stokes equations describe the fluid dynamics–Stokes equations, presented in vector form as:

$$\rho \left(\frac{\partial \vec{V}}{\partial t} + \vec{V} . \nabla \vec{V} \right) = -\nabla p + \mu \nabla^2 \vec{V} \tag{4}$$

where ρ is the fluid density (kg/m^3), μ is the dynamic viscosity ($kg/m \cdot s$), and p is the pressure (N/m^2). These equations are solved in conjunction with the energy equation to evaluate heat transfer performance under the specified boundary conditions.

To account for thermal effects, the model includes the energy conservation equation, as the system is heated from below. The energy equation governing heat transfer in the fluid domain is expressed as:

$$\nabla . \left(\rho C_p \vec{V} T \right) = \nabla . (k \nabla T) \tag{5}$$

where C_p is the specific heat capacity of the fluid ($J/kg \cdot K$), k is the thermal conductivity ($W/m \cdot K$), and T is the temperature (K). This equation describes the convective and conductive heat transfer within the fluid.

The solid regions of the model, comprising the TPMS structure and the heated base block, are treated separately. In the current experimental setup, the TPMS geometry is made of copper, while the heated base block is fabricated from aluminum. Heat conduction within these solid materials is governed by the steady-state heat conduction equation (Laplace equation), given by:

$$\nabla . (k_s \nabla T) = 0 \tag{6}$$

where k_s represents the thermal conductivity of the solid material, which can be either copper or aluminum, depending on the region.

The boundary conditions applied to the numerical model are defined as follows:

- Inlet Velocity Condition: A uniform inlet velocity $u = u_{in}$ is prescribed in the x-direction at the channel entrance. Three different flow rates of 11.8 cm^3/s, 15.73 cm^3/s and 19.85 cm^3/s where both experimentally and numerically. These flow rates correspond to inlet velocities of 0.15 m/s, 0.2 m/s and 0.25 m/s, respectively.
- Inlet Temperature Condition: The fluid enters the domain with a prescribed temperature $T = T_{in}$, which varies slightly depending on the experimental conditions but is approximately 10.5 °C.
- Outlet Boundary Condition: An open boundary is applied at the outlet, where all normal stresses are set to zero, allowing for fully developed flow to exit the domain without artificial pressure buildup.
- Thermal Boundary Condition: All external surfaces of the computational domain are assumed to be adiabatic, implying no heat loss to the surroundings. This is implemented using a Neumann boundary condition such that $\frac{\partial T_s}{\partial n} = 0$, where n is the outward normal vector to the surface.

Figure 7 illustrates the computational domain and the corresponding boundary conditions applied in the numerical simulation.
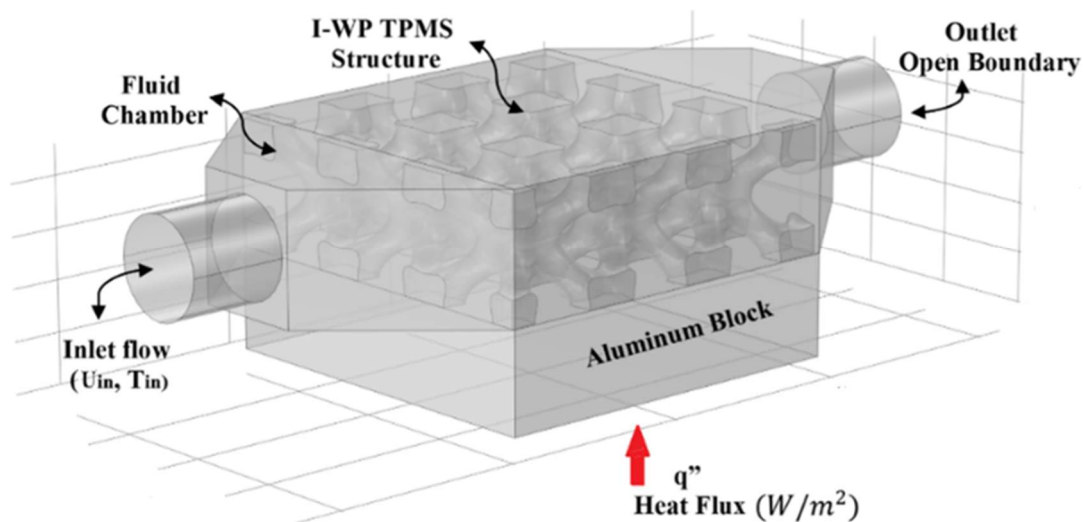

Figure 7. Boundary conditions.

3.1.2. Mesh Sensitivity Analysis and Convergence Criteria

Mesh sensitivity analysis is essential to ensure the accuracy and reliability of the numerical results. Table 4 summarizes the various mesh configurations adopted in COMSOL Multiphysics®, where unstructured tetrahedral elements are employed throughout the geometry including the edges, boundaries, and interior domain. Each mesh level is characterized by its total number of elements, and the average Nusselt number is used as the primary indicator for assessing mesh independence. For this analysis, the inlet velocity is set to $u_{in} = 0.15$ m/s, and the inlet temperature is $T = 10.5$ °C. A uniform heat flux of 38.4 kW/m^2, consistent with the experimental setup, is applied to the heated surface.

As shown in Table 4, the results indicate that Normal mesh is the suitable mesh size to be used. However, if one examines the Nusselt number for the coarse mesh and the normal mesh, the difference in Nusselt number is 0.32. Thus, to save in computation time, a coarse mesh is used for this case. Thus, balancing computational efficiency and precision.

Table 4. Mesh sensitivity analysis.

Mesh Level	Total Number of Elements	Nu$_{avg}$
Extra Coarse	79,981	82.27
Coarser	147,133	65.35
Coarse	322,152	61.18
Normal	888,322	60.86

A segregated solver approach is employed to decouple and solve the governing equations. The convergence criteria are imposed on all primary variables, including velocity components, pressure, and temperature, such that the solution is considered converged when the residuals fall below 1×10^{-6} between successive iterations. Figure 8 illustrates the mesh structure applied in the numerical model, highlighting the spatial distribution and refinement of the tetrahedral elements.
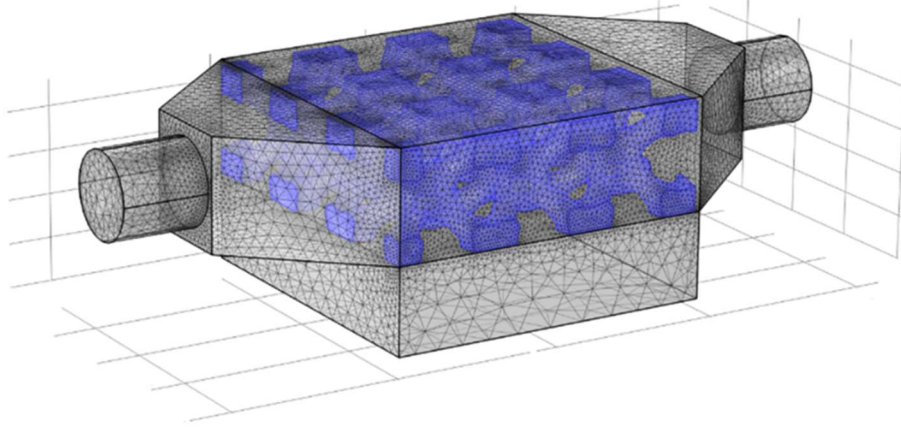

Figure 8. Mesh model containing 322,152 elements.

3.1.3. Relevant Non Dimensional Parameters

The dimensionless local Nusselt number (N_u) used in this study is defined as:

$$N_u = \frac{hD_H}{k} \tag{7}$$

where h is the local convective heat transfer coefficient $(W/m^2 . K)$, D_H is the hydraulic diameter (m), and k is the thermal conductivity of water $(W/m . K)$. The convective heat transfer coefficient is calculated using:

$$h = \frac{q''}{T - T_{in}} \tag{8}$$

In this formulation, q'' represents the applied heat flux (W/m^2), T_{in} is the inlet fluid temperature, and T is the temperature measured (or numerically evaluated) 1 mm below the interface between the TPMS structure and the heated base block. The hydraulic diameter is given by:

$$D_H = \frac{2H.W}{H + W} \tag{9}$$

where H and W are the height and width of the flow channel, respectively. For the current setup, the hydraulic diameter is calculated to be 17.86 mm.

The Reynolds number (R_e) is used to characterize the flow regime and is defined as:

$$R_e = \frac{\rho u_{in}D}{\mu} \tag{10}$$

Here, u_{in} is the inlet velocity (m/s), ρ is the fluid density (kg/m^3), μ is the dynamic viscosity $(kg/m.s)$, and D is the inlet cylinder diameter. Water is used as the circulating liquid. The Darcy friction factor (f) for the flow domain is computed using the following expression:

$$f = \frac{0.5\Delta pD_H}{\rho \, u_{in}^2 L} \tag{11}$$

where $\Delta p = p_{in} - p_{out}$ is the pressure drop across the domain, and L is the length of the heated region. To evaluate the overall thermal-hydraulic performance of the system, the PEC is employed. PEC combines both heat transfer enhancement and pressure drop penalty and is defined as:

$$PEC = \frac{N_{u_{avg}}}{f^{1/3}} \tag{12}$$

This non-dimensional metric provides an effective measure for comparing different flow and structural configurations by balancing thermal performance with hydraulic efficiency [19,20]. TPMS geometries were

generated using the MS-Lattice software developed by Al-Ketan [3], and their corresponding STL files are illustrated in Figure 9. For numerical–experimental correlation, unit cell sizes of 6 mm and 8 mm were modelled and compared with the experimental results presented in Table 2. This comparison enabled accurate calibration of the numerical model. Once validated, the calibrated model was employed to predict thermal performance for unit cell sizes of 10 mm, 12 mm, and 14 mm, specifically focusing on temperature distribution, local Nusselt number, and the PEC, as defined in Equation (12). An important parameter considered in this analysis is the total surface area of each TPMS structure, which is shown in Figure 9. As evident from the figure, the surface area decreases with increasing unit cell size. This geometric change has a direct influence on heat transfer characteristics and is critical for performance assessment. It is also noteworthy that all TPMS models used in the simulations represent solid networks, consistent with the experimental configurations. Among the tested geometries, the I-WP structure presents significant challenges in numerical modeling. Its complex geometry complicates mesh generation, necessitating careful meshing strategies to maintain solution stability and accuracy.

This led to an accurate calibration of the model. Then, for unit cells of 10 mm, 12 mm and 14 mm, the calibrated model is used to predict the temperature distribution and the heat enhancement by investigating the local Nusselt number and the performance evaluation criteria, as shown in Equations (7) and (12), respectively.
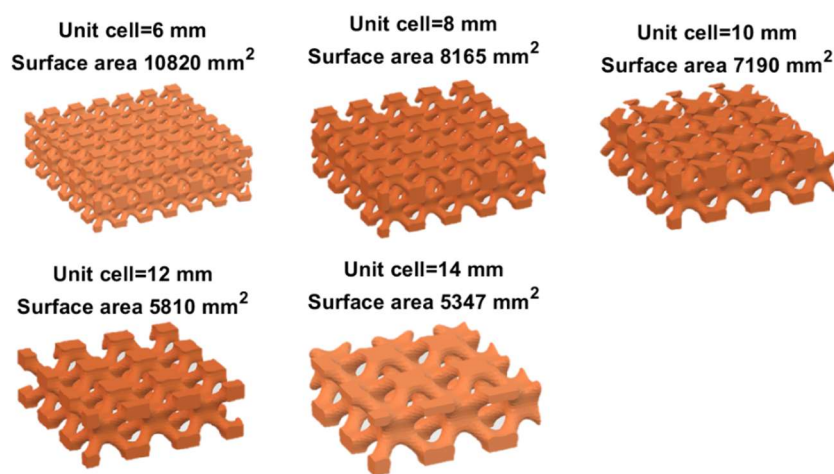

Figure 9. TPMS structure used for numerical simulation.

3.2. Comparison with Experimental Data

The set of governing equations described in Equations (3)–(6), comprising the continuity, momentum (Navier-Stokes), and energy equations, was solved using COMSOL Multiphysics®, which employs the finite element method to simulate coupled fluid flow and heat transfer within the TPMS domain. To ensure the accuracy and reliability of the simulation results, a mesh sensitivity study was conducted. This confirmed that the selected mesh resolution adequately captured the thermal and fluid dynamics without incurring excessive computational cost. To facilitate a direct and meaningful comparison with experimental data, temperatures were extracted from the numerical model at the exact locations where thermocouples were placed in the physical setup. The boundary conditions, including the inlet fluid temperature and applied heat flux, were set to match the experimental conditions precisely. This consistency between the numerical and experimental setups allowed for a robust validation of the model.

Figure 10 compares the numerically predicted and experimentally measured temperature profiles for three different flow rates: 11.8 cm^3/s, 15.75 cm^3/s and 19.85 cm^3/s, all corresponding to a unit cell size of 6 mm. As shown, there is a strong correlation between the two datasets. Both numerical and experimental results exhibit similar trends and slope characteristics along the flow direction, indicating that the model effectively captures the dominant heat transfer mechanisms occurring within the TPMS structure. The slight deviations observed between the two datasets are likely due to inherent uncertainties in the experimental measurements, including thermocouple calibration errors, heat losses to the environment, and minor fluctuations in flow rate control.

Despite these factors, the maximum temperature difference between the experimental and numerical results remains within 3%, as illustrated in Figure 10b. This level of agreement demonstrates the accuracy and robustness of the numerical model, confirming its suitability for predicting the thermal behaviour of TPMS-based heat exchangers under varying flow conditions.

The comparison between experimental and numerical results was further extended to the case with a unit cell size of 8 mm. As the unit cell size increases, the geometry becomes more open, resulting in reduced flow resistance and lower frictional losses. This effect improves flow uniformity and impacts the overall heat transfer performance. Figure 11 presents the temperature distribution for the 8 mm unit cell, in a format directly comparable to the results shown in Figure 10 for the 6 mm configuration. Once again, the numerical predictions align well with the experimental measurements, indicating that the calibrated model remains reliable across varying geometric configurations. To provide a comprehensive overview, Figure 12 summarizes the temperature distributions for all tested flow rates across both 6 mm and 8 mm unit cells. This comparison illustrates consistent trends between numerical and experimental data sets and confirms that the model accurately captures the influence of flow rate and geometric variation on the thermal response. The continued agreement reinforces the robustness and predictive capability of the numerical approach used in this study.
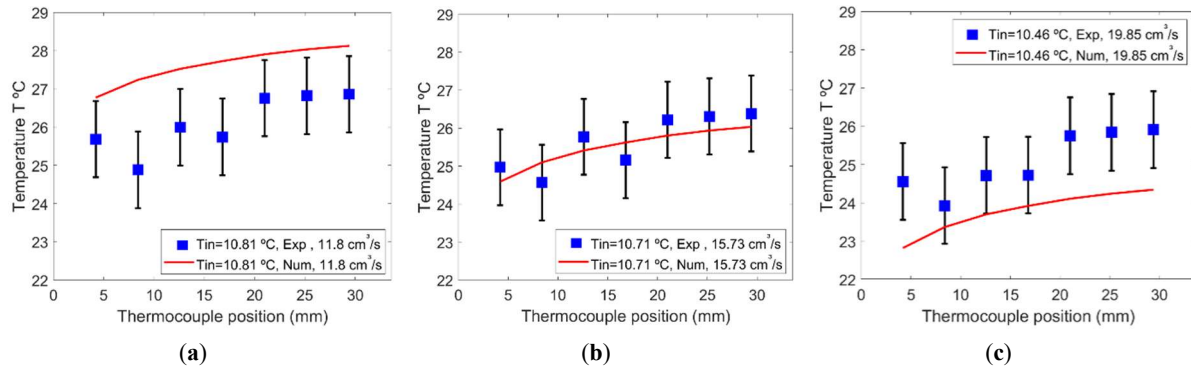

Figure 10. Temperature distribution along the flow for UC = 6 mm for different flow rates. (**a**) Flow rate = 11.8 cm^3/s; (**b**) 15.7 cm^3/s; (**c**) 19.6 cm^3/s.
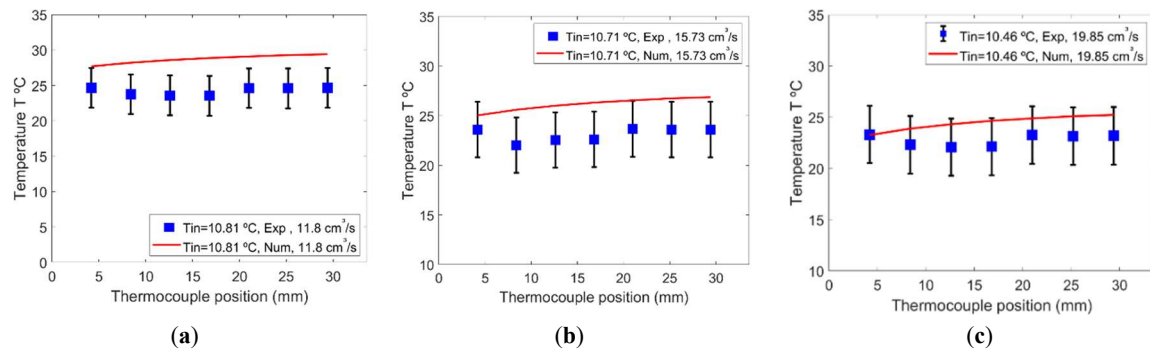

Figure 11. Comparison of the temperature between experiment and numerical calculation for UC = 8 mm. (**a**) Flow rate = 11.8 cm^3/s; (**b**) 15.7 cm^3/s; (**c**) 19.6 cm^3/s.

To further evaluate thermal performance, the local Nusselt number was calculated for both the 6 mm and 8 mm unit cell sizes, and the results are presented in Figure 13.
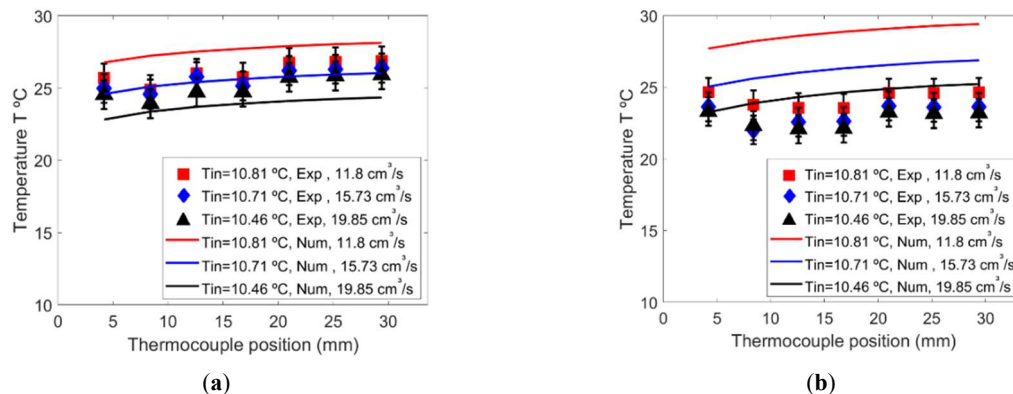

Figure 12. Comparison of the temperature between experiment and numerical calculation for all tested flow rates across both (**a**) UC = 6 mm and (**b**) UC = 8 mm.

It is important to note that even a 1 °C difference in temperature between the experimental and numerical datasets can lead to noticeable discrepancies in the Nusselt number.

This sensitivity is attributed to the way convective heat transfer is calculated, as outlined in Equations (7) and (8), where the temperature appears in the denominator of the expression for the convective heat transfer coefficient. Despite this sensitivity, the overall difference in local Nusselt number between the two data sets is approximately 7%. For clarity, the vertical axis (temperature or Nusselt number) in Figure 12 is scaled to illustrate these differences better. Nevertheless, the general trend and magnitude of the values show that a good agreement has been achieved, reinforcing the validity of the numerical model in predicting both temperature fields and convective heat transfer behaviour.
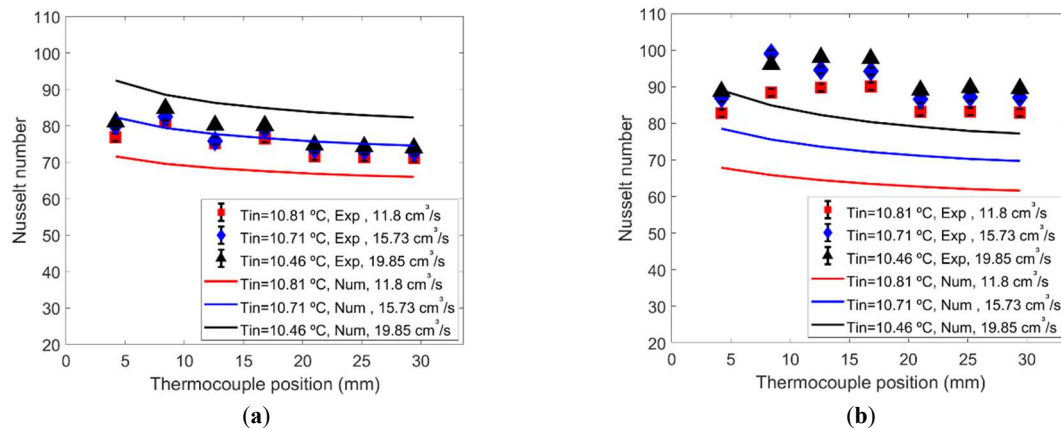

Figure 13. Comparison of the local Nusselt number between experiment and numerical calculation for UC = 6 mm. (**a**) UC = 6 mm; (**b**) UC = 8 mm.

For each case, the TPMS geometry was updated accordingly, as illustrated in Figure 9, reflecting the geometric variation inherent in changes to the unit cell size. The boundary conditions remained consistent with the validated model: the inlet velocity matched the flow rates previously used in both experimental and numerical analyses, and the inlet temperature was set to 10.5 °C, ensuring consistency across all simulations. Similarly, the applied heat flux was kept constant, equal to that used in earlier configurations.

Figure 14 presents the simulated temperature distributions for the three flow rates across the new unit cell sizes. A closer examination of the results reveals slight temperature fluctuations in the region near thermocouples 2, 3, and 4 for the 10 mm unit cell. Interestingly, these fluctuations are significantly diminished or absent in the simulations for the 12 mm and 14 mm unit cells.
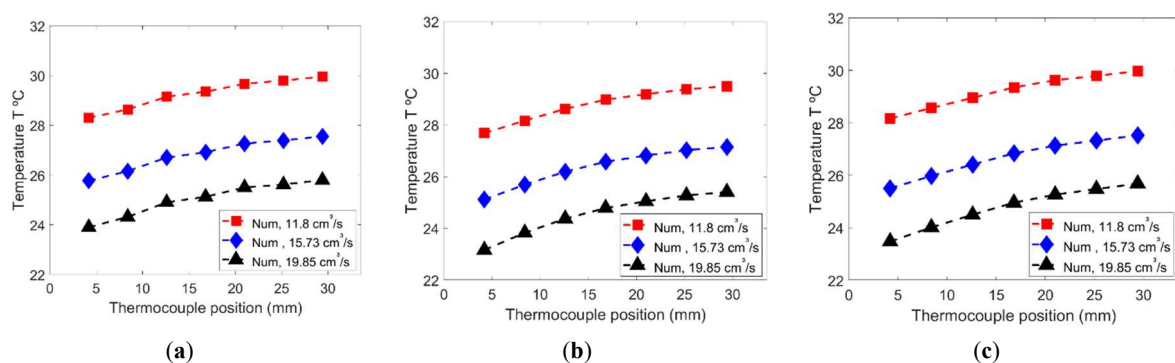

Figure 14. Numerical prediction of the temperature distribution for different flow rates and for additional unit cell sizes. (**a**) UC = 10 mm; (**b**) UC = 12 mm; (**c**) UC = 14 mm.

The results underscore the influence of TPMS geometry on thermal performance and confirm the model's capability to resolve subtle differences in heat transfer behaviour associated with structural variation. It is believed that minor structural deformation may occur in the TPMS geometry at the 10 mm unit cell size, which could contribute to irregularities in the thermal field. An interesting observation from the numerical results is that the thermal performance appears to be optimal when the unit cell size is 12 mm. Compared to the 10 mm and 14 mm cases, the 12 mm configuration consistently exhibits lower temperature magnitudes throughout the domain, indicating enhanced cooling effectiveness.

Figure 15 presents the computed local Nusselt number distributions for the three unit cell sizes. The previously observed temperature fluctuations in the 10 mm configuration are reflected in the local Nusselt number profile, where non-uniformities and local peaks are more pronounced.

In contrast, the 12 mm unit cell yields a smoother Nusselt distribution with higher average values, confirming superior convective heat transfer performance.
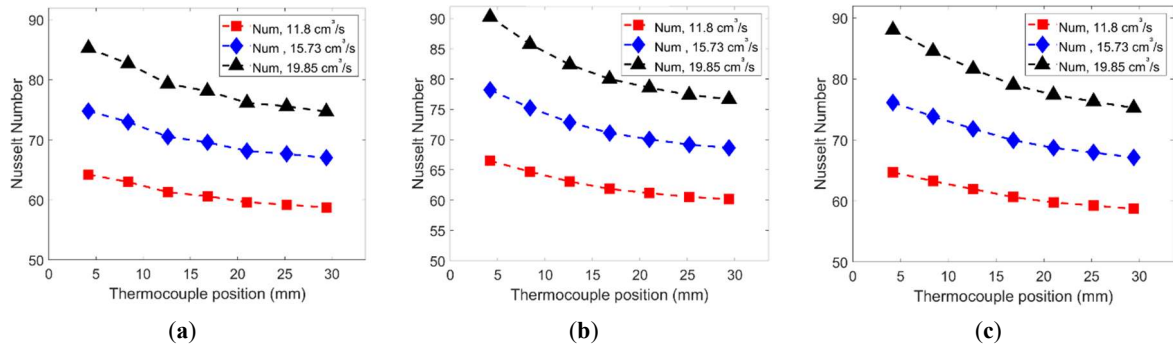

Figure 15. Numerical prediction of the local Nusselt number for different flow rates and for additional unit cell sizes. (**a**) UC = 10 mm; (**b**) UC = 12 mm; (**c**) UC = 14 mm.

Meanwhile, the 14 mm unit cell demonstrates reduced thermal performance, likely due to a decrease in surface area and reduced flow-structure interaction. These findings suggest that the 12 mm unit cell strikes a balance between flow accessibility and surface interaction, resulting in more efficient heat transfer. This highlights the importance of geometrical tuning in TPMS design to optimize cooling performance in thermofluidic applications. To further assess the superior performance observed with the TPMS configuration at a unit cell size of 12 mm, the PEC was calculated for all three unit cell sizes (10 mm, 12mm and 14 mm). The results clearly indicate that the PEC attains its highest value at 12 mm, highlighting this configuration as the most thermally efficient. Since PEC incorporates both convective heat transfer (through the Nusselt number) and flow resistance (via the Darcy friction factor), this result confirms that the 12 mm unit cell offers an optimal balance between thermal enhancement and hydraulic performance. Conversely, the performance drops noticeably for the 10 *mm* unit cell. This reduction is likely due to increased flow resistance and temperature non-uniformities, as previously discussed, which may be caused by local deformation or geometric complexity that affects flow distribution. Although an initial response surface model (RSM) was previously developed using a subset of data, the fitting procedure has now been extended to include all five tested unit cell sizes 6mm, 8mm, 10mm, 12 mm and 14 mm. This comprehensive dataset allows for a more general and reliable correlation. The new empirical formulation for predicting the average Nusselt number across the full range of unit cell sizes is presented in Equation (13):

$$
\begin{aligned}
N_{avg}^{-1.92} = 51.5 \times 10^{-4} &- 9 \times 10^{-5}\,UC - 23.48 \times 10^{-4}\,u_{in} - 12 \times 10^{-5}\,u_{in}\,UC \\
&+ 3.68 \times 10^{-7}UC^2 + 57.21 \times 10^{-4}\,u_{in}{}^2
\end{aligned}
\tag{13}
$$

where u_{in} is the inlet velocity in m/s, and UC is the unit cell size in mm. This expanded model provides a valuable design tool for optimizing TPMS-based cooling structures by simultaneously accounting for geometric and flow-related parameters. Equation 13 is valid for the following range of variable of $6\,mm \leq UC \leq 14\,mm$ and $0.15\,m/s \leq u_{in} \leq 0.25\,m/s$.

Finally, Figure 16 presents the PEC as a function of unit cell size for all investigated flow rates.

The results clearly illustrate how PEC varies with changes in geometry, capturing the combined effects of heat transfer enhancement and flow resistance. A peak in PEC is observed at a unit cell size of 12 mm across all flow rates, reaffirming that this configuration achieves the most efficient thermal-hydraulic performance. To generalize the trend, a curve fitting was applied to the PEC data using regression analysis. The fitted curve closely matches the computed values and provides an effective means of predicting performance over a range of unit cell sizes. This visualization illustrates that the unit cell size plays a crucial role in determining the overall system performance.
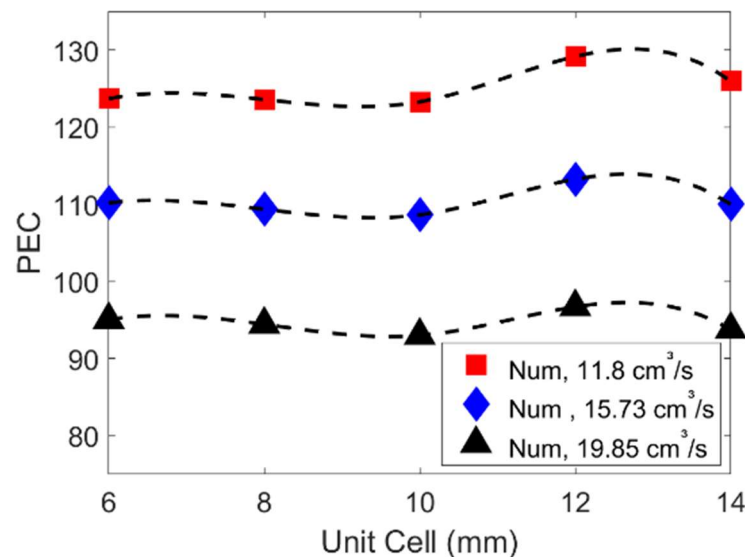
Figure 16. Performance evaluation criteria as a function of unit cell size for all flow rates.

4. Conclusions

TPMS is effective in cooling small surfaces such as heat sinks. This study experimentally and numerically investigated the thermal performance of Schoen's I-graph–Wrapped Package (I-WP) TPMS structure as a heat sink. The influence of unit cell size on convective heat transfer and flow resistance was the primary focus. A copper-based TPMS structure with a fixed porosity of 0.7 was designed using MSLattices and fabricated using 3D printing and tested under various flow conditions. Numerical simulations using COMSOL Multiphysics® were performed for a broader range of unit cell sizes to validate and extend the experimental findings. The experiment uses unit cell sizes of 4 mm, 6 mm and 8 mm, respectively. The problem is then solved numerically for a broader range of unit cells, from 4 mm to 14 mm. A comparison between experimental measurements and the numerical approach showed excellent agreement. The uniqueness of this investigation lies in its use of copper as a TPMS material and its variation of the unit cell size. An average Nusselt number correlation was developed from experimental data for unit cell sizes of 4 mm, 6 mm, and 8 mm, capturing the relationship between unit cell geometry and inlet velocity. A numerical model was successfully validated against experimental data, showing deviations of less than 3% for temperature and 7% for the local Nusselt number. This model was extended to unit cell sizes of 10 mm, 12 mm, and 14 mm, providing a broader predictive framework. The optimal thermal-hydraulic performance was observed at a unit cell size of 12 mm, as indicated by the highest PEC, demonstrating a balanced trade-off between convective enhancement and pressure drop. Both experimental and numerical results confirm that the I-WP structure supports uniform temperature distribution along the flow path, contrary to conventional metal foams with similar porosity, highlighting the potential of TPMS structures for efficient and compact heat exchanger design.

Overall, this study is among the first to experimentally validate the I-WP TPMS structure for thermal management, particularly in solid-network configurations. The findings highlight the significance of unit cell size in optimizing TPMS-based heat sinks and lay the groundwork for future research on geometrically tunable thermal systems utilizing additive manufacturing.

Author Contributions

M.Z.S: conceptualization, methodology, software; M.Y. and A.Y: data curation, writing—original draft preparation; M.Z.S, M.Y and A.Y.: visualization, investigation; M.Z.S.: supervision; M.Z.S, M.Y and A.Y.: software, validation; M.Z.S, M.Y and A.Y.: writing—reviewing and editing. All authors have read and agreed to the published version of the manuscript.

Funding

Institutional Review Board Statement

Not applicable.

Informed Consent Statement

Not applicable.

Data Availability Statement

Raw data available in Tables 2 and 3.

Conflicts of Interest

The authors declare no conflict of interest.

Use of AI and AI-Assisted Technologies

No AI tools were utilized for this paper.

Nomenclature

Nu_{avg}	Average Nusselt number
Nu	Local Nusselt number
T	Temperature in $^{\circ}$C
Tin	Inlet temperature ($^{\circ}$C)
W	TPMS structure width (mm)
H	TPMS structure height (mm)
u_{in}	Inlet velocity (m/s)
f	Friction coefficient
p	Pressure (N/m^2)
Δp	The pressure difference (N/m^2)
$D_H = \frac{2*(W*H)}{(W+H)}$	Hydraulic diameter (m)
D	Cylinder diameter (mm)
ρ	Fluid density (Kg/m^3)
μ	Fluid viscosity (Kg/m.s)
Cp	Fluid specific heat (J/kg.K)
k	Fluid conductivity (W/m.K)
UC	Unit cell in mm
q''	Heat flux normal to the bottom heated block (W/m^2)
Nu	Local Nusselt number
h	Heat transfer coefficient (W/m^2.K)
PEC	Performance Evaluation Criterion
Re	Reynolds number
L	TPMS structure length (mm)

References

1. Ahamed, M.K.; Wang, H.; Hazell, P.J. From biology to biomimicry: Using nature to build better structures–A review. *Constr. Build. Mater.* **2022**, *320*, 126195.

2. Ahmed, N.; Barsoum, I.; Abu Al-Rub, R.K. Numerical investigation on the effect of residual stresses on the effective mechanical properties of 3D-printed TPMS lattices. *Metals* **2022**, *12*, 1344.

3. Al-Ketan, O.; Abu Al-Rub, R.K. MSLattice: A free software for generating uniform and graded lattices based on triply periodic minimal surfaces. *Mater. Des. Process. Commun.* **2021**, *3*, e205.

4. Al-Ketan, O.; Al-Rub, R.K.A.; Rowshan, R. The effect of architecture on the mechanical properties of cellular structures based on the I-WP minimal surface. *J. Mater. Res.* **2018**, *33*, 343–359.

5. Baobaid, N.; Ali, M.I.; Khan, K.A.; et al. Fluid flow and heat transfer of porous TPMS architected heat sinks in free convection environment. *Case Stud. Therm. Eng.* **2022**, *33*, 101944.

6. Su, X.; Zhang, Y.; Rao, Y.; et al. Experimental and Numerical Study on Flow and Heat Transfer Characteristics of Additively Manufactured Triply Periodic Minimal Surface (TPMS) Heat Exchangers for Micro Gas Turbine. *Aerospace* **2025**, *5*, 416.

7. Wang, J.; Chen, K.; Zeng, M.; et al. Investigation on flow and heat transfer in various channels based on triply periodic minimal surfaces (TPMS). *Energy Convers.Manag.* **2023**, *283*, 116955.

8.   Tang, W.; Zhou, H.; Zeng, Y.; et al. Analysis on the convective heat transfer process and performance evaluation of Triply Periodic Minimal Surface (TPMS) based on Diamond, Gyroi (TPMS) based on Diamond, Gyroid and Iwp. *Int. J. Heat Mass Transf.* **2023**, *201*, 123642.

9.   Gandy, P.J.; Bardhan, S.; Mackay, A.L.; et al. Nodal surface approximations to the P, G, D and I-WP triply periodic minimal surfaces. *Chem. Phys. Lett.* **2001**, *336*, 187–195.

10. Kobayashi, Y.; Ohnuki, R.; Yoshioka, S. Discovery of I-WP minimal-surface-based photonic crystal in the scale of a longhorn beetle. *J. R. Soc. Interface* **2021**, *18*. https://doi.org/10.1098/rsif.2021.0505.

11. Montazerian, H.; Zhianmanesh, M.; Davoodi, E.; et al. Longitudinal and radial permeability analysis of additively manufactured porous scaffolds: Effect of pore shape and porosity. *Mater. Des.* **2017**, *122*, 146–156.

12. Tang, W.; Zou, C.; Guo, J.; et al. Experimental Investigation on the Convective Heat Transfer Performance of Five Triply Periodic Minimal Surfaces (TPMS): Gyroid, Diamond, Iwp, Primitive, and Fischer-Koch-S. *SSRN* **2023**. https://doi.org/10.2139/ssrn.4648952.

13. Zhang, C.; Qiao, H.; Yang, L.; et al. Vibration characteristics of additive manufactured IWP-type TPMS lattice structures. *Compos. Struct.* **2024**, *327*, 117642.

14. Men, Z.; Chen, W.; Li, Q.; et al. Topology optimization of the I-WP triply periodic minimal surfaces (TPMS) heat sink based on porous media effective model. *Int. J. Heat Mass Transf.* **2025**, *240*, 126657.

15. Rajkumar, R.; Ramkumar, J.; Balani, K. Design of TPMS-based Uniform and Hybrid Graded Lattice Structures: A Fluid Flow Analysis. *MATEC Web Conf.* **2024**, *401*, 11001.

16. Qureshi, Z.A.; Al-Omari, S.A.B.; Elnajjar, E.; et al. Using triply periodic minimal surfaces (TPMS)-based metal foams structures as skeleton for metal-foam-PCM composites for thermal energy storage and energy management applications. *Int. Commun. Heat Mass Transf.* **2021**, *124*, 105265.

17. Ouda, M.; Al-Ketan, O.; Sreedhar, N.; et al. Novel static mixers based on triply periodic minimal surface (TPMS) architectures. *J. Environ. Chem. Eng.* **2020**, *85*, 104289.

18. Yeranee, K.; Rao, Y. A review of recent investigations on flow and heat transfer enhancement in cooling channels embedded with triply periodic minimal surfaces (TPMS). *Energies* **2022**, *15*, 8994.

19. Saghir, M.Z.; Yahya, M.; Ortiz, P.D.; et al. Heat Enhancement of Ethylene Glycol/Water Mixture in the Presence of Gyroid TPMS Structure: Experimental and Numerical Comparison. *Processes* **2025**, *13*, 228.

20. Saghir, M.Z.; Yahya, M. Convection Heat Transfer and Performance Analysis of a Triply Periodic Minimal Surface (TPMS) for a Novel Heat Exchanger. *Energies* **2024**, *17*, 4275.

21. *COMSOL Software, Version 6.2*; COMSOL, Inc.: Burlington, MA, USA, 2024.